Surfaces and Interfaces 39 (2023) 102964

Contents lists available at ScienceDirect

Surfaces and Interfaces

journal homepage: www.sciencedirect.com/journal/surfaces-and-interfaces

Adsorption and X-ray photoelectron spectroscopy investigation of bisphosphonates on titania and hydroxyapatite surfaces

Leonardo Francisco Gonçalves Dias [a,*], Milena Yumi Kasama Nakata [a], Gabriel Junior Cavalcante Pimentel [a], Erika Soares Bronze-Uhle [b], Valmor Roberto Mastelaro [c], Paulo Noronha Lisboa-Filho [a]

[a] São Paulo State University – UNESP, School of Sciences, Bauru, São Paulo 17033360, Brazil
[b] Bauru School of Dentistry, São Paulo University – USP, Bauru, São Paulo 17012901, Brazil
[c] São Carlos Institute of Physics, São Paulo University – USP, São Carlos, São Paulo 13566590, Brazil

ARTICLE INFO

Keywords:
Adsorption
Surface characterization
Bisphosphonate
Titania
Hydroxyapatite

ABSTRACT

This study investigates the adsorption of bisphosphonates (BPs) on TiO_2, hydroxyapatite (HA), and TiO_2+HA composite surfaces. We first examined the adsorption of these molecules on titania particles and explored the influence of UV irradiation through adsorption curves. Our findings indicate that surface irradiation leads to an increase in the adsorbed BP content due to enhanced BP deprotonation and hydroxyl group generation. Additionally, we evaluated the adsorption of BPs on the TiO_2, HA, and TiO_2+HA surfaces primarily through X-ray photoelectron spectroscopy (XPS). Our results suggest that BPs adsorb onto TiO_2 via a condensation reaction between the BPs and titania surfaces, while phosphate and Ca^{2+} ions coordinate onto HA surfaces. All functionalized films exhibit a water contact angle of zero. Atomic force microscopy (AFM) measurements show that BP adsorption had less impact on titania topography than HA topography, and mixed films demonstrated behavior similar to that of titania films.

1. Introduction

Biomedical implants require consideration of both mechanical properties and surface characteristics [1]. To modify surface properties such as wettability, biocompatibility, and antibacterial activity, thin film production and organic molecule adsorption have been extensively studied [2–5].

Titanium dioxide (TiO_2) has been extensively studied for surface modifications and implant coatings due to its ability to adhere well to metallic substrates and the presence of hydroxyl groups on its surface [6]. However, TiO_2 is less biocompatible than hydroxyapatite (HA), which is a key component of human bone but poorly adheres to metallic substrates [7,8]. Thus, TiO_2+HA composite films have been developed to improve biocompatibility and adhesion to metallic substrates [9,10]. Moreover, these surfaces can be functionalized with different compounds ranging from amphiphilic molecules to proteins to improve their biological performance [3,11,12].

Bisphosphonates (BPs), an organic pyrophosphate analog, are a class of organic molecules employed for treating osseous diseases, and their linear structures are presented in Fig. 1 [13,14]. While most studies have focused on the biological performance of BPs, they have also been shown to increase osteoblast metabolic activity while inhibiting osteoclast, thereby promoting new bone formation [13,15,16].

BPs have a strong affinity for HA due to their ability to coordinate with calcium ions [13,17]. Thus, different studies, from theoretical calculations to measured adsorptions, have been conducted on the interaction of BPs with HA [18–21]. However, few studies have focused on the TiO_2/BP system [2,5,22]. When BPs interact with HA, phosphate groups in HA may be replaced by BP phosphonate groups, and/or calcium ions may coordinate with BP anions [23]. In contrast, BPs can adsorb onto TiO_2 through phosphonate groups, forming mono- or bidentate Ti–O–P bonds [2,5,22].

Therefore, we measured etidronate and alendronate BP adsorption on anatase and rutile TiO_2 to determine the influence of UV irradiation on adsorption and explore the effects of etidronate, alendronate, and risedronate on TiO_2, HA, and composite films. To the best of our knowledge, this is the first study to report a TiO_2+HA/BP system and generate adsorption curves for BPs on oxidized surfaces. The samples

* Corresponding author.
E-mail address: goncalves.dias@unesp.br (L.F.G. Dias).

https://doi.org/10.1016/j.surfin.2023.102964
Received 5 September 2022; Received in revised form 2 May 2023; Accepted 13 May 2023
Available online 20 May 2023

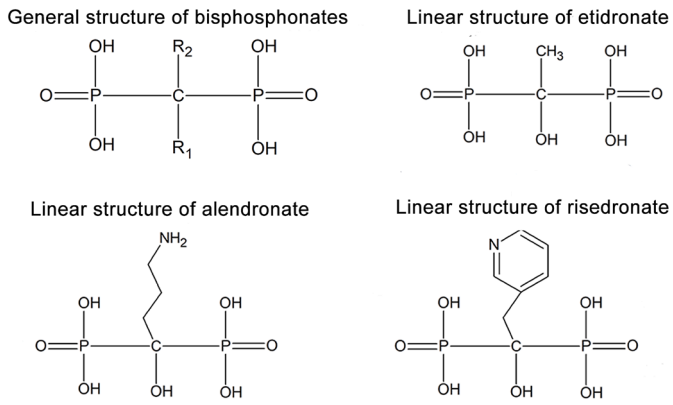

Fig. 1. Linear structures of BPs, etidronate, alendronate, and risedronate.

were investigated by X-ray diffraction (XRD), confocal microscopy, scanning electron microscopy (SEM), measuring water contact angles, X-ray photoelectron spectroscopy (XPS), and atomic force microscopy (AFM). Our findings could accelerate the development of biomedical implants with superior biocompatibility, wettability, and antibacterial activity. Besides, it helps to elucidate the understanding of the properties of surfaces-containing bisphosphonates.

2. Materials and methods

2.1. Materials

For sol–gel synthesis, titanium (IV) isopropoxide (Sigma–Aldrich®/CAS 546–68–9) and nitric acid (65%; Synth®/CAS 7697–37–2) were employed as precursors. The adsorptions of disodium etidronate hydrate (TCI® German/CAS 7414–83–7), sodium alendronate trihydrate (TCI® German/CAS 121268–17–5), and sodium risedronate (Sigma–Aldrich®/CAS 115436–72–1) were investigated. Hereinafter, etidronate, alendronate, and risedronate are referred to as "ETI," "ALE," and "RIS," respectively. KCl (NEON/CAS 7447–40–7) was employed to prepare the adsorption medium. H_2SO_4 (98%; Meta química/CAS 7664–93–9) and H_2O_2 (35%; Dinâmica/CAS 7722–84–1) were used to prepare the piranha solution. Cerium sulfate IV tetrahydrate (CAS 10294–42–5) was purchased from NEON® and was used as an oxidizing agent for quantifying BP absorption.

2.2. Synthesis of TiO_2 dispersion, HA, and TiO_2 particles

Titanium dioxide dispersion was synthesized as described by Trino et al. [24]. For synthesizing HA particles, we employed the procedure described by Ben-Arfa et al. [25]. TiO_2 nanoparticles were synthesized using the same procedure as that for preparing the TiO_2 dispersion, except the dispersion was left to dry completely instead of evaporating to 50 mL. The remaining powder was manually macerated using a pestle and a mortar. Anatase and rutile titania nanoparticles were formed by heating the powder at 1°C min^{-1} to 450 and 850°C, respectively, where the samples were held for 2 h and subsequently cooled to 1°C min^{-1}.

2.3. Preparation of Ti substrates and film deposition

Commercial pure titanium IV (Ti Cp IV, 12 mm diameter x 3 mm height) was used as the film deposition substrate. First, the substrates were laser-treated, as described by Borcherding et al. [26]. The surface was then cleaned using piranha solution (H_2SO_4:H_2O_2, 7:3 v/v) for 2 h. Finally, the substrates were ultrasonically cleaned with water and acetone for 10 min each and then dried at 60°C before deposition.

Four dispersions were prepared for film deposition. To prepare the titania films, the pristine TiO_2 dispersion was diluted in isopropanol (1:3 v/v). The hydroxyapatite dispersion was prepared by mixing 300 mg of HA powder with 6 mL of ethylene glycol. The product was then stirred for 15 min at 60°C. Then, 106 μL of Triton™-X and 1 mL of isopropanol were added, and the product was stirred for 15 min. Finally, the dispersion was ultrasonicated for 10 min. The final dispersions comprised mixtures of 1:1 and 1:2 volume/volume TiO_2 and HA dispersion, respectively (i.e., TiO_2:HA 1:1 and TiO_2:HA 1:2, in sequence). Finally, isopropanol was added at a ratio of 3:1 v/v TiO_2.

The films were deposited by spin-coating at 2000 rpm for 60 s. Before spinning, three drops of the desired dispersion were placed on the substrate. After 60 s, the films were dried at 60°C for 5 min. This procedure was repeated three times. The spin-coated films were heated at 1°C min^{-1} to 850°C where they were held for 2 h and then cooled at 1°C min^{-1}.

2.4. BP adsorption

We determined calibration curves for ETI and ALE solutions. The linearity regime was between 0 and 2 mM, representing the adsorption curve values for which the equilibrium concentration (Ceq) was < 2 mM. In each experiment, different ETI and ALE solution concentrations were prepared, usually 0.2 to 4 mM. For the adsorption test, 5 mg of titanium dioxide was left undisturbed to react with 1000 μL of the BP solution, and all experiments were performed in triplicate. First, the saturation time was determined, and the system was left undisturbed without stirring for 1, 2, or 3 h, then the absorbance was measured to check changes in concentration after the evaluated time. The saturation time was 2 h.

For the films, before functionalization, they were irradiated with ultraviolet (UV)-C (254 nm) light from an 8 W lamp for 45 min to increase the number of OH groups on and clean the surface [2]. For functionalization, 3 mL of the BP solution (4 mM in 1mM KCl) was left to react with each disk for 2 h, and the disk was then rinsed for 5 seconds in distilled water to remove any residual BP solution.

2.5. Characterizations

The crystallinity of the prepared materials was evaluated using XRD (D/MAX-2100/PC, Rigaku) equipped with a CuKα radiation source ($\lambda =$ 1.54056 Å) coupled to a nickel filter to eliminate CuKβ radiation. The samples were scanned from 10 to 100° (between the incident beam and the detector) in regular steps of 2 min^{-1} and 40 kV/20 mA. Diffractograms of TiO_2 particles are available in Fig. S1.

The UV absorbance was quantified using a Shimadzu UV-1800 spectrophotometer. A 0.5 M aqueous H_2SO_4 solution was used for preparing a 0.1% w/v cerium sulfate solution, as reported by Taha et al. [27]. The prepared cerium solution was stored in an amber-colored flask. Cerium sulfate exhibits a characteristic signal at 320 nm, and BP oxidation weakens the signal. The presented values are the absorbance multiplied by -1. The BP absorption was measured by placing 250 μL of the BP solution in a 15-mL tube and adding 2000 μL of cerium solution. The mixture was left to react without stirring for 1 h, and 6000 μL of 0.5 M H_2SO_4 was then added. The absorbance was measured by placing 1000 μL of the final product in a cuvette. The same procedure was adopted using a blank for generating a calibration curve by replacing the BP solution with a 1 mM KCl solution. BPs were adsorbed on the titania by adding 5 mg of nanoparticles to 1000 μL of the BP solution, then the mixture was manually shaken for 5 seconds. After the established time of 2 hours, the microtubes were centrifuged for 10 min at 10,000 rpm. An aliquot (250 μL) was removed using the same procedure. Although the same nanoparticle mass was used as a blank, the BP volume was replaced with an equal volume of 1 mM KCl. We employed CAVS software (freely available at http://www.prppg.ufpr.br/site/posalim/pb/aplicativos/) for model fitting. For the modeling the initial values of K_f and n were set to be equal to 0.1, then the software fitted a curve. The fitting was chosen based on the best R^2.

The specific surface area was determined using Micromeritics ASAP-2020. Nitrogen adsorption/desorption isotherms were measured at 77 K, and the surface area was calculated using the Brunauer–Emmett–-Teller (BET) method. Before the measurements, the samples were degassed at 70°C for 24 h. For particle size calculation (d), it was assumed that particles are spherical and the following equation was applied $d = 6 / A_s \rho$. Where A_s is the specific surface area and ρ is the density of the particles [28,29].

To capture microroughness and 3D images, a confocal microscope (Leica DCM3D) equipped with a 10 × lens was used. Root-mean-square (RMS) surface roughnesses were measured for three points in each sample.

SEM images were obtained using a Zeiss LS15 microscope operating at an acceleration voltage of 15 kV. The chemical composition was verified using energy-dispersive X-ray spectroscopy (EDS) for at least two distinct points on each sample, the accelerating voltage was 30 kV with an FWHM of 150 eV and a spot size of 1 μm.

Water contact angles were measured under ambient conditions using a goniometer (Ramé-Hart 100–00, Succasunna, NJ) and the sessile drop technique. A drop (5 μL) was automatically released over the film. For each sample, two drops were placed in different regions. For each drop, ten water contact angles were calculated using image processing, and the mean angle and standard deviation were calculated.

The chemical compositions of the material surfaces were determined using XPS (Scienta Omicron ESCA) equipped with an EA125 Xm1000 monochromator and an Al Kα (1486.7 eV) X-ray source. The survey spectra were collected using a pass energy of 50 eV and an energy step of 0.500 eV. High-resolution spectra were obtained using a pass energy of 30 eV and an energy step of 0.050 eV. A charge neutralizer (CN10) was used to exclude the surface charging effects. The spectra were fitted using CasaXPS software, and the binding energy was corrected using the aliphatic hydrocarbon C 1 *s* reference signal at 285.0 eV. The atomic surface concentration was evaluated based on Scofield's relative sensitivity factor (RSF).

The surface nanotopography and nanoroughness of the prepared samples were analyzed using AFM (Park XE7; Park Systems, Santa Clara, CA, USA) operating in the noncontact mode. A silicon cantilever (PPP-NCHR; Park Systems, Inc.) was employed at a constant force of 42.0 N m^{-1} and a frequency of 330 kHz. Measurements were performed in air at 20°C. Images (1 × 1 μm^2) were scanned at 0.7 Hz.

3. Results and discussion

When applied as a surface modifier, BPs can increase cell growth [2,12,30]. Therefore, studying their adsorption on TiO_2, which is usually the composition of the outermost bioimplant layer, may help to develop more biocompatible surfaces. We investigated the adsorption of BPs on different surfaces. On particles, we employed ETI and ALE on anatase and rutile surfaces, and we evaluated the effect of UV irradiation on BP adsorption. Our results indicated that UV irradiation is an effective method for increasing BP adsorption. We extensively characterized TiO_2 and HA film surfaces and found that BPs adsorbed on the surface were exposed to P–OH groups, leading to a water contact angle of 0°.

3.1. Effects of BP adsorption on TiO_2 particles

The BET measurements are presented in Table 1. From these results, although anatase titania has a higher surface area than rutile titania, the latter has larger pores that can influence the adsorption capacity, as the molecules can go inside the pores. The anatase and rutile titania comprised nanoparticles and microparticles, respectively, which was expected because we did not control the rutile particle growth. Findings obtained by X-ray diffraction are presented in Fig. S1.

Table 1
BET measurements of prepared samples.

	Anatase	Rutile
BET surface area ($m^2 g^{-1}$)	92.6	2.4
Pore width (Å)	60.1	534.5
Nanoparticle size (nm)	64.8	2521.6

From the UV–Vis measurements, we obtained parameters for the Freundlich adsorption model, as listed in Table 2. In the Freundlich model, *N* is related to the heterogeneity of the system. If the number is higher than one, it means that the adsorption is more heterogeneous. The parameter *K* is the adsorption capacity or affinity constant, and R^2 is the coefficient of determination from the fitting [31]. The results showed that UV irradiation increased the affinity of BPs for titania surfaces, which was verified by the increased affinity constant (*K*). ETI had a higher affinity for anatase, while ALE for rutile, respectively.

The adsorption curves are presented in Fig. 2. All the curves show that the surface adsorption increased when the surface was exposed to UV irradiation. The effect of UV irradiation on adsorption was previously described by our group [2], and the influence of hydroxylation on phosphonic acid adsorption was investigated in another study [32]. In our previous study, we observed that UV exposition predominantly affected the adsorption of phosphonate groups. In this study, we complement this result by determining that in general UV exposure increases adsorption on the titania surface.

Phosphonate adsorbs on TiO_2 through deprotonation of H_2PO_3 groups. Deprotonation increases BP reactivity, and HPO_3^- or PO_3^{2-} reacts with Ti–O on the surface, forming Ti–O–P bonds [5]. BPs are mostly attached through bidentate bonds, exposing the additional phosphate and other groups of the molecule [32], which suggests that UV irradiation (which may increase the number of OH groups) increases the BP deprotonation as BPs approach the surface. Thus, the surface OH rapidly recombined with H^+ from the H_2PO_3 groups, forming Ti–O–P bonds. This would also explain the predominant adsorption on Ti surfaces, which decreases the Ti^{3+} content owing to the generation of Ti–OH groups, which favors H_2PO_3 condensation with the surface.

3.2. Structures, composition, and morphologies of prepared films

For the structural analyses, we dried the deposition solutions following the heating procedure described in Section 2.2. The results are shown in Fig. 3. The spectrum for pure titanium dioxide presented rutile characteristic peaks (PDF No. 2–494), while pure HA presented its expected structure (PDF No. 3–747). The spectra for the composite materials exhibited rutile, HA, and anatase (PDF No. 21–1272) characteristic peaks. With an increasing HA content, the HA peak intensified.

Table 3 lists the mean surface roughness of the prepared samples measured by confocal microscopy. The film deposition decreased the surface roughness by approximately 35% compared with the pristine sample, and the HA film exhibited the lowest surface roughness. The standard deviation also reduced compared with pure Ti, indicating that the film deposition increased the surface homogeneity. Several studies have attempted to determine the relationship between the (nano/micro) surface roughness and cellular activity [33–35]. The corresponding confocal images are shown in Fig. S2.

SEM (based on secondary electrons) was employed to investigate the

Table 2
Freundlich adsorption parameters obtained from experimental data.

Sample	*N*	*K* ((mg g^{-1})(L mg^{-1}))	R^2
ETI on anatase	1.0 ± 0.1	0.2 ± 0.1	0.995
UV + ETI on anatase	2.6 ± 0.2	13.1 ± 1.7	0.988
ETI on rutile	0.6 ± 0.1	0.1 ± 0.1	0.937
UV + ETI on rutile	1.8 ± 0.2	4.5 ± 1.9	0.928
ALE on anatase	5.2 ± 1.1	18.0 ± 4.5	0.873
UV + ALE on anatase	2.3 ± 0.6	4.6 ± 2.9	0.908
ALE on rutile	2.0 ± 0.7	4.9 ± 2.0	0.937
UV + ALE on rutile	5.0 ± 1.1	40.3 ± 10.1	0.927

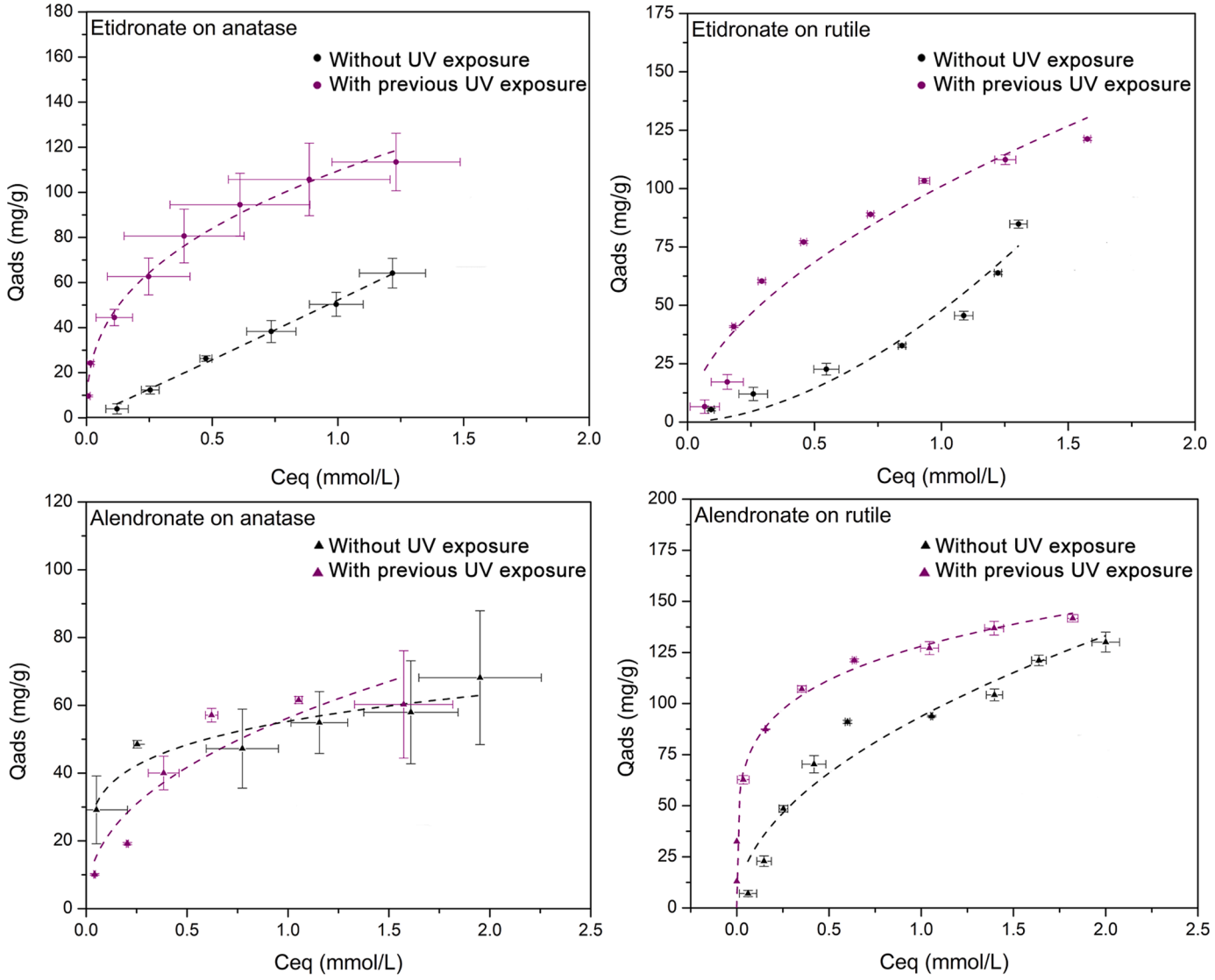

Fig. 2. Adsorption curves of BP adsorbed on titania particles. Dotted lines represent theoretical curves.

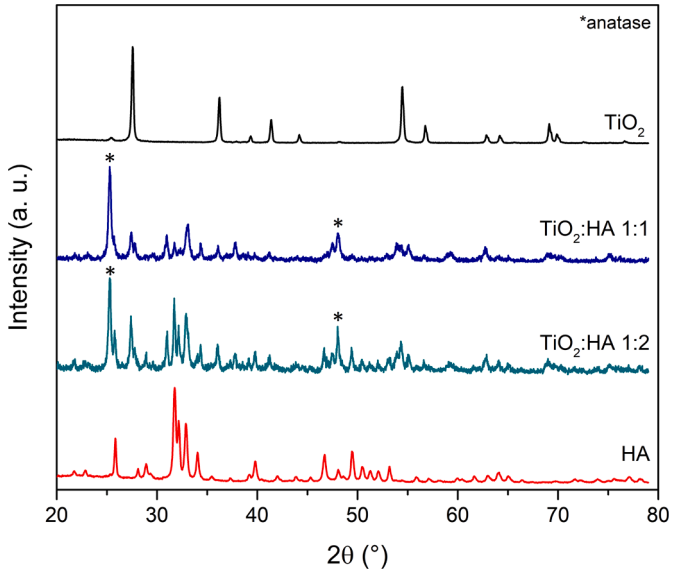

Fig. 3. XRD patterns of dried dispersions.

Table 3
Mean surface roughness of prepared samples.

Sample	Mean Surface Roughness (μm)
Ti	41.7 ± 1.6
TiO_2	37.7 ± 0.4
TiO_2:HA 1:1	28.9 ± 0.7
TiO_2:HA 1:2	35.4 ± 0.7
HA	27.8 ± 0.5

surface morphology, and the SEM images of the prepared films are presented in Fig. 4. At low magnifications, the TiO_2 surface appears smooth compared with the other surfaces. Cracks are common on HA-containing films [32] and are attributed to mechanical constraints during heating. Only the TiO_2:HA 1:1 film exhibited cracks. The titania and HA surfaces comprised small cubes and rod-like particles, respectively, the composite film surfaces exhibited both particles.

The EDS measurements are listed in Table 4, and the corresponding elemental composition maps are shown in Figures S3–S6. Calcium and phosphorus were homogeneously distributed on the surface, except for the HA sample, where it was possible to observe regions with higher concentrations. HA and TiO_2:HA 1:1 had Ca/P ratios close to 1.67. TiO_2:HA 1:2 presented a low value of phosphorous compared with the other

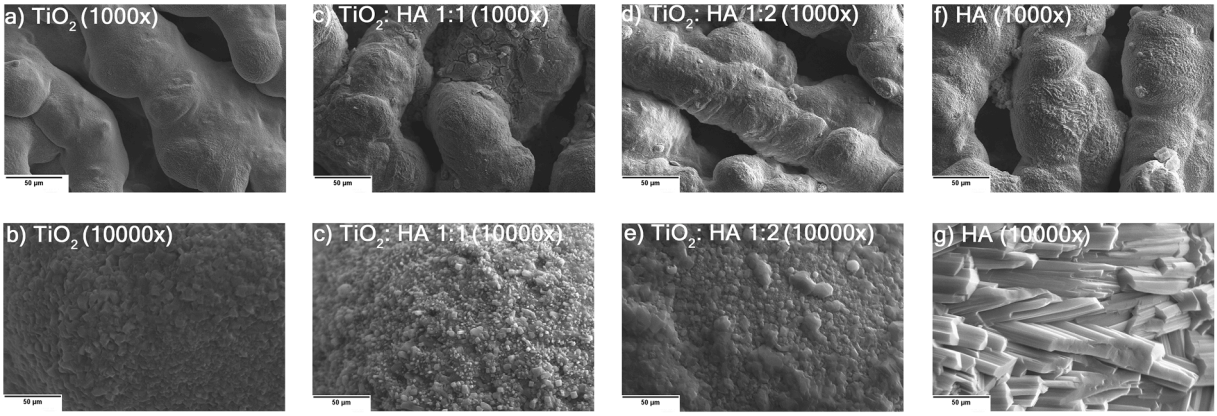

Fig. 4. SEM images of prepared samples.

Table 4
Elements in atomic% measured by EDS.

Sample	Elements (at%)			
	Ti	O	Ca	P
TiO_2	28.2 ± 1.9	71.7 ± 1.9	-	-
TiO_2:HA 1:1	28.3 ± 0.4	65.1 ± 0.1	3.7 ± 1.2	2.0 ± 0.1
TiO_2:HA 1:2	26.8 ± 0.7	66.8 ± 2.9	4.1 ± 1.8	1.3 ± 0.7
HA	2.5 ± 0.2	62.2 ± 2.6	16.0 ± 2.0	9.0 ± 0.4

samples, and once the HA came from the same dispersion of the TiO_2:HA 1:1 sample, this difference was not expected.

3.3. *Effects of BPs adsorption on TiO_2, HA, and TiO_2+HA films*

Surface hydrophilicity was evaluated by varying the concentration of BPs. For this, we measured samples functionalized with 0.2 mM and 4 mM solutions. The results demonstrated that small concentrations had the same effect on hydrophilicity at a concentration of 4 mM. Table 5 presents only the results for the 4 mM samples; further results are presented in Table S1. Since the 0.2 mM and 4 mM samples showed similar results, we focused our investigation on the 4 mM samples.

The results obtained for TiO_2 differed from those obtained for smooth TiO_2 [5]. The water contact angle did not show any decrease after BP adsorption (1 mM) in the referred study. This indicates a synergetic effect between the roughness and BP layers. This behavior suggests that our samples follow Wenzel's model: once the substrate has a water contact angle lower than 90°, an increase in roughness leads to an increase in hydrophilicity [36,37]. The pure HA film presented a lower water contact angle than that in the published results [38,39]. After the adsorption of BP, the water drops completely spread on the surface. The addition of HA to TiO_2 appears to be beneficial, especially for the TiO_2:HA 1:1 sample, which completely spread the drop, even in the absence of BPs.

XPS was used to examine the surface composition in detail, and the results are presented in the following sections. Table 6 presents the atomic concentrations of the studied surfaces obtained from survey measurements. BPs were successfully adsorbed on TiO_2 because of the presence of phosphorous in these samples. Additionally, an increase in nitrogen content due to the presence of nitrogen-containing BPs was observed. For samples of pure or HA, the presence of BPs was observed due to an increase in phosphorous concentration and the presence of nitrogen on the surface for nitrogen-containing bisphosphonates. For TiO_2:HA 1:1, the decrease in phosphorus was attributed to the substitution of phosphates on HA by phosphates of BPs.

The C 1 s high-resolution spectra of the prepared films are displayed in Fig. 5. We added contributions (286.2 eV) from P_2C–O moieties, based on the presence or increase in phosphorous concentration. This strategy follows previous investigations on bulk phosphonic acids [5,11,40]. The higher peaks are centered at approximately 285.0, 286.6, and 288.8 eV, for aliphatic carbon, C–O, and O–C=O, respectively [11]. A few samples showed a contribution centered at 286.0 eV from C–N; for TiO_2, TiO_2/ETI, and TiO_2:HA 1:1 samples, this was attributed to contamination (a peak at approximately 400.0 eV was observed in the N 1 s

Table 5
Water contact angle (WCA) for pristine and samples prepared with 4 mM BP solutions.

Samples	WCA (°)
TiO_2	49.7 ± 8.2
TiO_2/ETI	0*
TiO_2/ALE	0*
TiO_2/RIS	0*
TiO_2:HA 1:1	0*
TiO_2:HA 1:1/ETI	0*
TiO_2:HA 1:1/ALE	0*
TiO_2:HA 1:1/RIS	0*
TiO_2:HA 1:2	34.7 ± 1.9
TiO_2:HA 1:2/ETI	0*
TiO_2:HA 1:2/ALE	0*
TiO_2:HA 1:2/RIS	0*
HA	37.5 ± 2.5
HA/ETI 4 mM	0*
HA/ALE 4 mM	0*
HA/RIS 4 mM	0*

* 0 indicates that the water drop was completely spread on the surface.

Table 6
Surface elementary composition from XPS measurements.

Sample	Elements (at%)					
	C 1*s*	O 1*s*	N 1*s*	Ti 2*p*	Ca 2*p*	P 2*p*
TiO_2	32.9	50.1	1.9	15.1	-	-
TiO_2/ETI	45.1	40.6	1.8	10.4	-	2.2
TiO_2/ALE	51.8	33.8	3.9	6.1	-	4.4
TiO_2/RIS	64.3	26.6	2.2	6.2	-	0.7
TiO_2:HA 1:1	29.1	49.8	-	13.4	4.1	3.7
TiO_2:HA 1:1/ETI	39.8	43.3	1.2	11.9	1.3	2.5
TiO_2:HA 1:1/ALE	40.1	42.8	1.4	10.1	1.3	4.2
TiO_2:HA 1:1/RIS	31.2	46.6	1.8	10.8	4.6	5.0
TiO_2:HA 1:2	28.3	50.9	-	14.7	3.6	2.5
TiO_2:HA 1:2/ETI	44.6	39.4	-	9.8	2.5	3.8
TiO_2:HA 1:2/ALE	34.7	47.7	0.8	11.0	2.8	3.0
TiO_2:HA 1:2/RIS	28.6	49.1	1.4	11.6	4.7	4.7
HA	50.3	35.0	-	8.4	4.5	1.7
HA/ETI	27.4	51.6	-	12.5	4.3	4.2
HA/ALE	35.2	42.6	0.6	8.3	6.1	7.2
HA/RIS	41.1	35.6	3.2	5.3	6.2	8.6

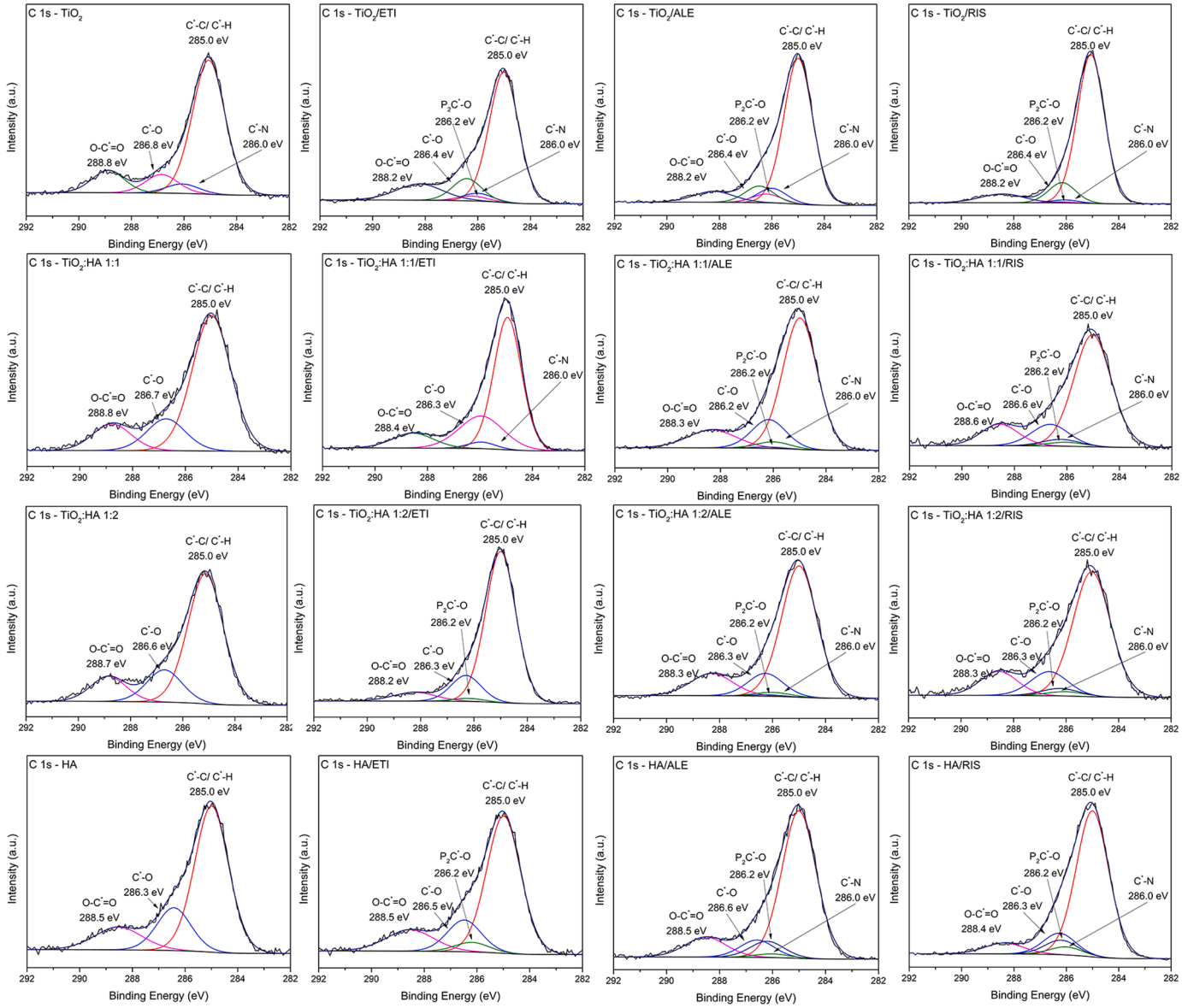

Fig. 5. C 1 *s* high-resolution XPS spectra of prepared films. BP (4 mM) was employed for functionalization.

high-resolution spectra – see Fig. S7) [11,41,42]. In other samples, this peak is due to the presence of nitrogen-containing BPs (see Fig. S7). It is possible to observe a decrease in the carboxyl groups on the TiO_2 samples compared with pristine titania, which is consistent with previous results and indicates competitive adsorption [5]. Pure HA samples did not exhibit a decrease in carboxyl groups, similar to pure TiO_2. This is consistent with the adsorption mechanism of BPs on HA surfaces because BPs adsorb on HA mainly through the coordination of Ca^{2+} ions and $-PO_3^{-2}$ moieties [20].

The O 1 s high-resolution spectra of the prepared films are displayed in Fig. 6. All the spectra show a peak centered at approximately 530 eV from TiO_2 [43]. The spectra of molecules adsorbed on TiO_2 were fitted based on the bulk octadecylphosphonic acid and etidronate contributions [5,11]. For the three adsorbents on TiO_2, we detected contributions at approximately 531.2 eV from organic oxygen, P=O, and Ti–O–P, and at approximately 532.7 eV from P–OH from free phosphonic acid moieties [22,41,44]. These results suggest that BPs adsorb equally on rough and smooth titania through the condensation of phosphonates and Ti–OH groups.

Without BPs, samples of pure or containing HA present three peaks. In addition to TiO_2, which is centered around 529.8 eV, the peaks are centered at approximately 531.0 eV from organic oxygen, phosphates, and hydroxyl groups [45–47]; the third peak, centered at approximately 532.7 eV was attributed to free P–OH groups from HA [47]. In the presence of BPs, the same peaks were observed; however, in some samples, there was an increase in the peak centered at 531.0 eV, which was attributed to an increase in the number of $-PO_3^{-2}$ groups due to BP adsorption and the formation of Ti-O-P bonds. The Ca 2p and P 2p spectra were omitted. Fig. S7 shows the N 1 s high-resolution spectra of the nitrogen-containing samples. We observed a contribution at approximately 400 eV from C-N contributions and one from positively charged nitrogen at approximately 401.4 eV [48].

We accessed the surface nano topography using AFM, and the results are displayed in Fig. 7, together with the RMS roughness. For rough TiO_2, no increase in surface roughness was observed, which is different from the reported results [2,5,49]. Except for TiO_2:HA 1:1/ETI, no increase in surface roughness after BP adsorption was observed. Even a small increase was expected since it has been reported to increase in HA [50].

Previously, we hypothesized that on a smooth surface, BPs follow the

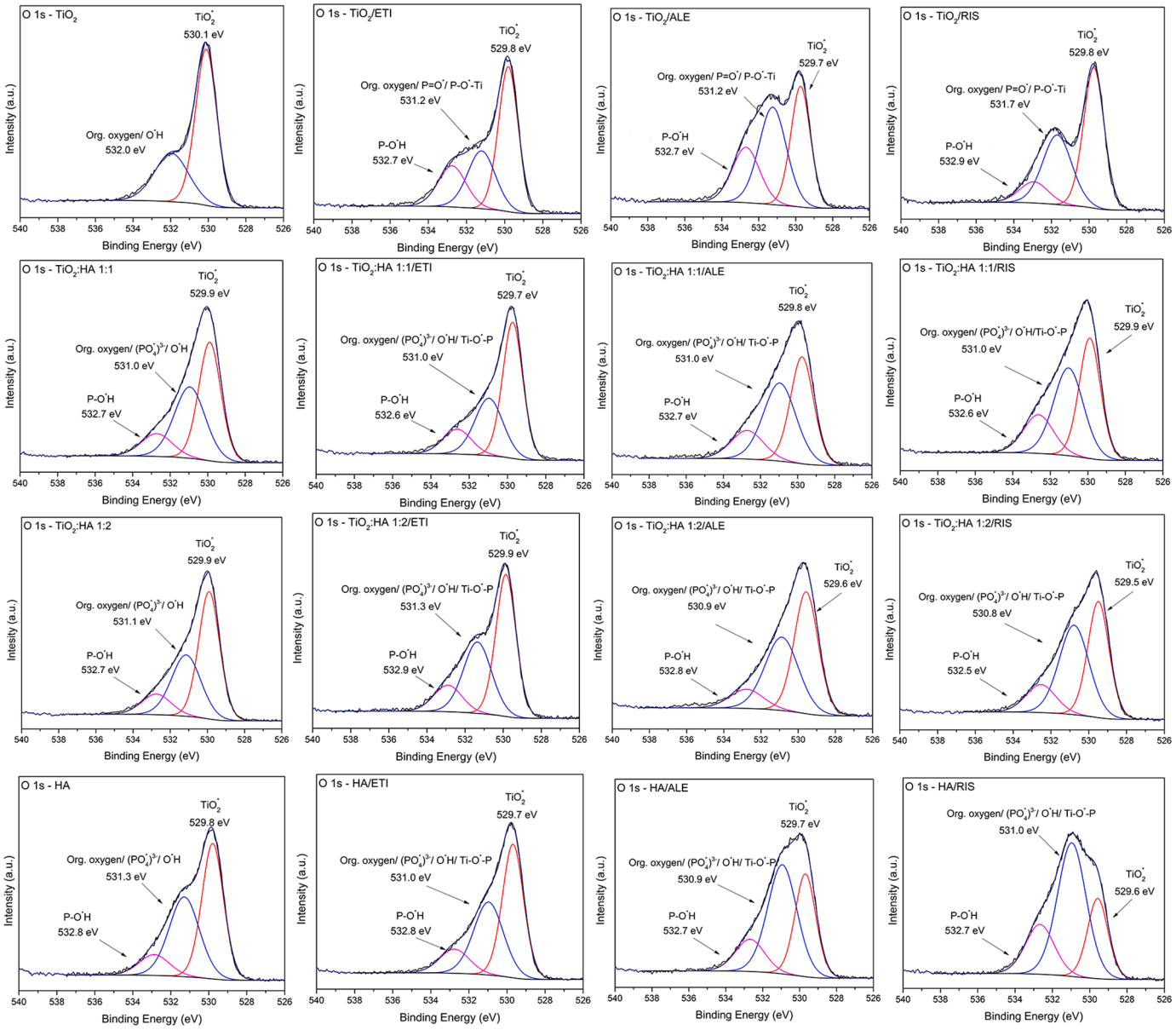

Fig. 6. O 1 *s* high-resolution XPS spectra of prepared films. BP (4 mM) was employed for functionalization.

surface topography, while on rough surfaces, they approximate the molecules and increase localized adsorption [5]. However, we did not observe an increase in TiO_2 roughness samples after BP adsorption, which suggests that our hypothesis needs to be reformulated. Our new inference is that, in general, BPs may adsorb following TiO_2 topography, while HA surfaces approximate molecules, increasing adsorption through charge interactions.

4. Conclusion

The present study provides insights into the adsorption behavior of BPs on TiO_2 particles, TiO_2, HA, and TiO_2+HA films. The results demonstrate that the adsorption of BPs on TiO_2 particles follows the Freundlich model, with the affinity constant of etidronate and alendronate showing opposite trends between anatase and rutile Moreover, UV irradiation of titania was found to increase the amount of adsorbed on the surface of the particle and changes its affinity. Our hypothesis that the increase of hydroxyl groups on the titania surface would increase the deprotonation of BPs and lead to higher levels of adsorption was supported by the experimental results. These findings contribute to a better understanding of the underlying mechanism of BP adsorption on TiO_2 particles, which is essential for the development of new therapeutic strategies.

The investigation of BP adsorption on TiO_2, HA, and TiO_2+HA films revealed successful film formation and provided valuable insights into the surface properties of the films. The results from XRD, confocal microscopy, SEM, water contact angle, XPS, and AFM showed that the films had different surface properties, which affected the adsorption behavior of BPs. The complete spread of the water drop on the surface after BPs adsorption and the presence of phosphorus and nitrogen in some samples indicated successful adsorption of the molecules. Interestingly, surface roughness increased only for HA surfaces, suggesting that charge effects play a crucial role in BP adsorption on surfaces. To further our understanding of the influence of hydroxylation on adsorption, future studies should include theoretical investigations along with biological evaluations of similar systems. Overall, our results provide important insights into the adsorption behavior of BPs on different surfaces, which has implications for the development of new drug delivery systems.

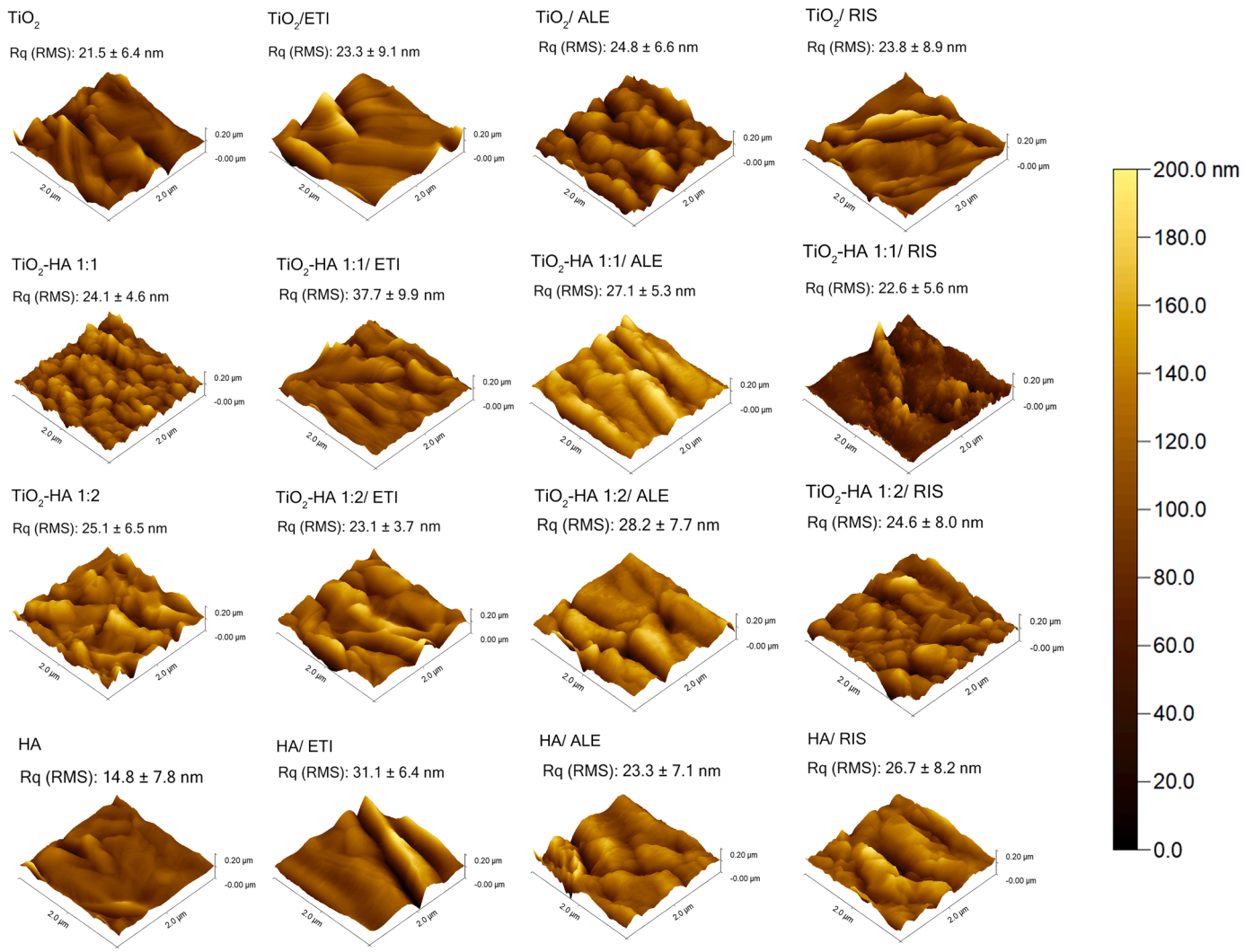

Fig. 7. AFM images of prepared samples. BP (4 mM) was used for functionalization.

Declaration of Competing Interest

The authors declare that they have no known competing financial interests or personal relationships that could have appeared to influence the work reported in this paper.

Data availability

Data will be made available on request.

Acknowledgments

This work was financially supported by the São Paulo Research Foundation FAPESP through grants 2018/07520–3, and 2013/07296–2. The authors acknowledge Marina Honorato for her helpful comments and study critique, Giseli Sina for designing the graphical abstract, and LaPTec for water-contact-angle measurements.

Supplementary materials

Supplementary material associated with this article can be found, in the online version, at doi:10.1016/j.surfin.2023.102964.

References

[1] B.D. Ratner, D.G. Castner, Surface Properties and Surface Characterization of Biomaterials, Fourth Edi. (2020), https://doi.org/10.1016/b978-0-12-816137-1.00006-4.
[2] E.S. Bronze-Uhle, L.F.G. Dias, L.D. Trino, A.A. Matos, R.C. de Oliveira, P.N. Lisboa-Filho, Physicochemical bisphosphonate immobilization on titanium dioxide thin films surface by UV radiation for bio-application, Surf. Coat. Technol. 357 (2019) 36–47, https://doi.org/10.1016/j.surfcoat.2018.09.038.
[3] E.S. Bronze-Uhle, L.F.G. Dias, L.D. Trino, A.A. Matos, R.C. de Oliveira, P.N. Lisboa-Filho, Physicochemical characterization of albumin immobilized on different TiO2 surfaces for use in implant materials, Colloids Surf. A Physicochem. Eng. Asp. 564 (2019) 39–50, https://doi.org/10.1016/j.colsurfa.2018.12.028.
[4] L.D. Trino, L.F.G. Dias, L.G.S. Albano, E.S. Bronze-Uhle, E.C. Rangel, C.F.O. Graeff, P.N. Lisboa-Filho, Zinc oxide surface functionalization and related effects on corrosion resistance of titanium implants, Ceram. Int. 44 (2018) 4000–4008, https://doi.org/10.1016/j.ceramint.2017.11.195.
[5] L.F.G. Dias, J.P.C. Rheinheimer, O.P. Gomes, M. Noeske, S. Stamboroski, E. S. Bronze-Uhle, M.C. Mainardi, W.L. Cavalcanti, A.B. Neto, P.N. Lisboa-Filho, Bisphosphonates on smooth TiO 2 : modeling and characterization, ChemistrySelect 7 (2022), https://doi.org/10.1002/slct.202200286.
[6] T. Hanawa, Titanium-tissue interface reaction and its control with surface treatment, Front. Bioeng. Biotechnol. 7 (2019), https://doi.org/10.3389/fbioe.2019.00170.
[7] J.Y. Han, Z.T. Yu, L. Zhou, Hydroxyapatite/titania composite bioactivity coating processed by sol-gel method, Appl. Surf. Sci. 255 (2008) 455–458, https://doi.org/10.1016/j.apsusc.2008.06.072.
[8] W.S.W. Harun, R.I.M. Asri, J. Alias, F.H. Zulkifli, K. Kadirgama, S.A.C. Ghani, J.H. M. Shariffuddin, A comprehensive review of hydroxyapatite-based coatings adhesion on metallic biomaterials, Ceram. Int. 44 (2018) 1250–1268, https://doi.org/10.1016/j.ceramint.2017.10.162.

[9] X. Wang, B. Li, L. Zhou, J. Ma, X. Zhang, H. Li, C. Liang, S. Liu, H. Wang, Influence of surface structures on biocompatibility of TiO2/HA coatings prepared by MAO, Mater. Chem. Phys. 215 (2018) 339–345, https://doi.org/10.1016/j.matchemphys.2018.05.037.

[10] G. He, J. Hu, S.C. Wei, J.H. Li, X.H. Liang, E. Luo, Surface modification of titanium by nano-TiO 2 /HA bioceramic coating, Appl. Surf. Sci. 255 (2008) 442–445, https://doi.org/10.1016/j.apsusc.2008.06.088.

[11] L.F. Gonçalves Dias, S. Stamboroski, M. Noeske, D. Salz, K. Rischka, R. Pereira, M. do C. Mainardi, M.H. Cardoso, M. Wiesing, E.S. Bronze-Uhle, R.B. Esteves Lins, P.N. Lisboa-Filho, New details of assembling bioactive films from dispersions of amphiphilic molecules on titania surfaces, RSC Adv. 10 (2020) 39854–39869, https://doi.org/10.1039/D0RA06511K.

[12] C.S. Albano, A. Moreira Gomes, G. da Silva Feltran, C.J. da Costa Fernandes, L. D. Trino, W.F. Zambuzzi, P.N. Lisboa-Filho, Biofunctionalization of titanium surfaces with alendronate and albumin modulates osteoblast performance, Heliyon 6 (2020) e04455, https://doi.org/10.1016/j.heliyon.2020.e04455.

[13] A.M.A. Menezes, F.A.C. Rocha, H.v. Chaves, C.B.M. Carvalho, R.A. Ribeiro, G.A. C. Brito, Effect of sodium alendronate on alveolar bone resorption in experimental periodontitis in rats, J. Periodontol. 76 (2005) 1901–1909, https://doi.org/10.1902/jop.2005.76.11.1901.

[14] M.J. Rogers, J. Mönkkönen, M.A. Munoz, Molecular mechanisms of action of bisphosphonates and new insights into their effects outside the skeleton, Bone 139 (2020), 115493, https://doi.org/10.1016/j.bone.2020.115493.

[15] R.G.G. Russell, P.I. Croucher, M.J. Rogers, Bisphosphonates: pharmacology, mechanisms of action and clinical uses, Osteoporo. Int. 9 (1999) 66–80, https://doi.org/10.1007/PL00004164.

[16] Y. Cui, T. Zhu, D. Li, Z. Li, Y. Leng, X. Ji, H. Liu, D. Wu, J. Ding, Bisphosphonate-functionalized scaffolds for enhanced bone regeneration, Adv. Healthc. Mater. 8 (2019) 1–21, https://doi.org/10.1002/adhm.201901073.

[17] S. Chen, R. Guo, C. Xie, Q. Liang, X. Xiao, Biomimetic mineralization of nanocrystalline hydroxyapatites on aminated modified polylactic acid microspheres to develop a novel drug delivery system for alendronate, Mater. Sci. Eng. C 110 (2020), https://doi.org/10.1016/j.msec.2020.110655.

[18] L. Forte, S. Sarda, C. Combes, F. Brouillet, M. Gazzano, O. Marsan, E. Boanini, A. Bigi, Hydroxyapatite functionalization to trigger adsorption and release of risedronate, Colloids Surf. B Biointerfaces 160 (2017) 493–499, https://doi.org/10.1016/J.COLSURFB.2017.09.055.

[19] L. Forte, S. Sarda, P. Torricelli, C. Combes, F. Brouillet, O. Marsan, F. Salamanna, M. Fini, E. Boanini, A. Bigi, Multifunctionalization modulates hydroxyapatite surface interaction with bisphosphonate: antiosteoporotic and antioxidative stress materials, ACS Biomater. Sci. Eng. 5 (2019) 3429–3439, https://doi.org/10.1021/acsbiomaterials.9b00795.

[20] C. Chen, M. Xia, L. Wu, C. Zhou, F. Wang, Modeling the interaction of seven bisphosphonates with the hydroxyapatite(100) face, J. Mol. Model. 18 (2012) 4007–4012, https://doi.org/10.1007/s00894-012-1398-z.

[21] H. Aghabozorg, B. Sohrabi, S. Mashkouri, H.R. Aghabozorg, Ab initio DFT study of bisphosphonate derivatives as a drug for inhibition of cancer: NMR and NQR parameters, J. Mol. Model. 18 (2012) 929–936, https://doi.org/10.1007/s00894-011-1114-4.

[22] Ž. Petrović, A. Šarić, I. Despotović, J. Katić, R. Peter, M. Petravić, M. Petković, A new insight into coating's formation mechanism between TiO2 and alendronate on titanium dental implant, Materials (2020) 13, https://doi.org/10.3390/ma13143220.

[23] B. Palazzo, M. Iafisco, M. Laforgia, N. Margiotta, G. Natile, C.L. Bianchi, D. Walsh, S. Mann, N. Roveri, Biomimetic hydroxyapatite-drug nanocrystals as potential bone substitutes with antitumor drug delivery properties, Adv. Funct. Mater. 17 (2007) 2180–2188, https://doi.org/10.1002/adfm.200600361.

[24] L.D. Trino, E.S. Bronze-Uhle, A. George, M.T. Mathew, P.N. Lisboa-Filho, Surface physicochemical and structural analysis of functionalized titanium dioxide films, Colloids Surf. A Physicochem. Eng. Asp. 546 (2018) 168–178, https://doi.org/10.1016/j.colsurfa.2018.03.019.

[25] B.A.E. Ben-Arfa, I.M.M. Salvado, J.M.F. Ferreira, R.C. Pullar, Novel route for rapid sol-gel synthesis of hydroxyapatite, avoiding ageing and using fast drying with a 50-fold to 200-fold reduction in process time, Mater. Sci. Eng. C 70 (2017) 796–804, https://doi.org/10.1016/j.msec.2016.09.054.

[26] K. Borcherding, D. Marx, L. Gätjen, N. Bormann, B. Wildemann, U. Specht, D. Salz, K. Thiel, I. Grunwald, Burst release of antibiotics combined with long-term release of silver targeting implant-associated infections: Design, characterization and in vitro evaluation of novel implant hybrid surface, Materials 12 (2019) 1–13, https://doi.org/10.3390/ma122333838.

[27] E.A. Taha, N.F. Youssef, Spectrophotometric determination of some drugs for osteoporosis, Chem. Pharm. Bull. (Tokyo) 51 (2003) 1444–1447, https://doi.org/10.1248/cpb.51.1444.

[28] J.H.G. Rangel, P.R.G. Gonçalves, M.M. Oliveira, M.I.B. Bernardi, E. Longo, L.E. B. Soledade, I.M.G. Santos, A.G. Souza, Nanometric Pb1-xLaxTiO3 (x = 0, 0.13 and 0.27) powders obtained by the polymeric precursor method, Mater. Res. Bull. 43 (2008) 825–835, https://doi.org/10.1016/j.materresbull.2007.05.005.

[29] V.D. Araújo, J.D.A. Bellido, M.I.B. Bernardi, J.M. Assaf, E.M. Assaf, CuO-CeO2 catalysts synthesized in one-step: Characterization and PROX performance, Int. J. Hydrogen Energy 37 (2012) 5498–5507, https://doi.org/10.1016/j.ijhydene.2011.12.143.

[30] H.S. Kim, J.I. Lee, S.S. Yang, B.S. Kim, B.C. Kim, J. Lee, The effect of alendronate soaking and ultraviolet treatment on bone–implant interface, Clin. Oral. Implants Res. 28 (2017) 1164–1172, https://doi.org/10.1111/clr.12933.

[31] S.O. Lesmana, N. Febriana, F.E. Soetaredjo, J. Sunarso, S. Ismadji, Studies on potential applications of biomass for the separation of heavy metals from water and wastewater, Biochem. Eng. J. 44 (2009) 19–41, https://doi.org/10.1016/j.bej.2008.12.009.

[32] R. Luschtinetz, A.F. Oliveira, H.A. Duarte, G. Seifert, Self-assembled monolayers of alkylphosphonic acids on aluminum oxide surfaces - A theoretical study, Z. Anorg. Allg. Chem. 636 (2010) 1506–1512, https://doi.org/10.1002/zaac.201000016.

[33] P. Mazón, D. García-Bernal, L. Meseguer-Olmo, F. Cragnolini, P.N. de Aza, Human mesenchymal stem cell viability, proliferation and differentiation potential in response to ceramic chemistry and surface roughness, Ceram. Int. 41 (2015) 6631–6644, https://doi.org/10.1016/j.ceramint.2015.01.110.

[34] K. Rafiee, H. Naffakh-Moosavy, E. Tamjid, The effect of laser frequency on roughness, microstructure, cell viability and attachment of Ti6Al4V alloy, Mater. Sci. Eng. C 109 (2020), https://doi.org/10.1016/j.msec.2020.110637.

[35] A. Zareidoost, M. Yousefpour, B. Ghasemi, A. Amanzadeh, The relationship of surface roughness and cell response of chemical surface modification of titanium, J. Mater. Sci. Mater. Med. 23 (2012) 1479–1488, https://doi.org/10.1007/s10856-012-4611-9.

[36] D. Quéré, Wetting and roughness, Annu. Rev. Mater. Res. 38 (2008) 71–99, https://doi.org/10.1146/annurev.matsci.38.060407.132434.

[37] J. Wang, Y. Wu, Y. Cao, G. Li, Y. Liao, Influence of surface roughness on contact angle hysteresis and spreading work, Colloid. Polym. Sci. 298 (2020) 1107–1112, https://doi.org/10.1007/s00396-020-04680-x.

[38] N. Eliaz, S. Shmueli, I. Shur, D. Benayahu, D. Aronov, G. Rosenman, The effect of surface treatment on the surface texture and contact angle of electrochemically deposited hydroxyapatite coating and on its interaction with bone-forming cells, Acta Biomater. 5 (2009) 3178–3191, https://doi.org/10.1016/j.actbio.2009.04.005.

[39] W. Chen, S. Oh, A.P. Ong, N. Oh, Y. Liu, H.S. Courtney, M. Appleford, J.L. Ong, Antibacterial and osteogenic properties of silver-containing hydroxyapatite coatings produced using a sol gel process, J. Biomed. Mater. Res. A 82 (2007) 899–906, https://doi.org/10.1002/jbm.a.31197.

[40] I. Milošev, M. Metikoš-Huković, Ž. Petrović, Influence of preparation methods on the properties of self-assembled films of octadecylphosphonate on Nitinol: XPS and EIS studies, Mater. Sci. Eng. C 32 (2012) 2604–2616, https://doi.org/10.1016/j.msec.2012.08.010.

[41] C. Theile-Rasche, M. Wiesing, S. Schwiderek, M. Noeske, G. Grundmeier, How self-assembled organophosphonic acid monolayers on Ti0.5Al0.5 N hard coatings affect the adsorption of polycarbonate melt, Appl. Surf. Sci. 513 (2020), 145701, https://doi.org/10.1016/j.apsusc.2020.145701.

[42] J. Landoulsi, M.J. Genet, C. Richard, K. el Kirat, S. Pulvin, P.G. Rouxhet, Evolution of the passive film and organic constituents at the surface of stainless steel immersed in fresh water, J. Colloid Interface Sci. 318 (2008) 278–289, https://doi.org/10.1016/j.jcis.2007.09.087.

[43] P.E.; B.K.D. Moulder, J.F.;Stickle W.F.; Sobol, Handbook of X-ray Photoelectron Spectroscopy, 1993.

[44] V. Zoulalian, S. Zürcher, S. Tosatti, M. Textor, S. Monge, J.J. Robin, Self-Assembly of poly (ethylene glycol)-poly (alkyl phosphonate) terpolymers on titanium oxide surfaces: synthesis, interface characterization, investigation of nonfouling properties, and long-term stability, Langmuir 26 (2010) 74–82, https://doi.org/10.1021/la902110j.

[45] S. Jerdioui, L.L. Elansari, N. Jaradat, S. Jodeh, K. Azzaoui, B. Hammouti, M. Lakrat, A. Tahani, C. Jama, F. Bentiss, Effects of gallic acid on the nanocrystalline hydroxyapatite formation using the neutralization process, J. Trace Elem. Miner. 2 (2022), 100009, https://doi.org/10.1016/j.jtemin.2022.100009.

[46] E. Bolli, S. Kaciulis, A. Mezzi, V. Ambrogi, M. Nocchetti, L. Latterini, A. di Michele, G. Padeletti, Hydroxyapatite functionalized calcium carbonate composites with ag nanoparticles: An integrated characterization study, Nanomaterials (2021) 11, https://doi.org/10.3390/nano11092263.

[47] J. Bai, T. Nagashima, T. Yajima, XPS Study of Apatite Formed from Simulated Body Fluid on a Titanium Substrate Surface Nitrided by an Atmospheric Pressure Nitrogen Microwave Plasma, n.d.

[48] G. Beamson, D.; Briggs, High resolution XPS of organic polymers, the scienta ESCA300 database, 5 (1993) 778–778. 10.1002/adma.19930051035.

[49] D. Zheng, K.G. Neoh, E.T. Kang, Immobilization of alendronate on titanium via its different functional groups and the subsequent effects on cell functions, J. Colloid Interface Sci. 487 (2017) 1–11, https://doi.org/10.1016/j.jcis.2016.10.014.

[50] M. Othmani, A. Aissa, C.G. Bac, F. Rachdi, M. Debbabi, Surface modification of calcium hydroxyapatite by grafting of etidronic acid, Appl. Surf. Sci. 274 (2013) 151–157, https://doi.org/10.1016/j.apsusc.2013.03.002.